Visual Comput (2005) 21: 265–278
DOI 10.1007/s00371-005-0288-0

ORIGINAL ARTICLE

Gladimir V. G. Baranoski
Aravind Krishnaswamy
Bradley Kimmel

Increasing the predictability of tissue subsurface scattering simulations

Published online: 12 May 2005

G. V. G. Baranoski · A. Krishnaswamy · B. Kimmel
Natural Phenomena Simulation Group, School of Computer Science, University of Waterloo

Abstract Models of light interaction with matter usually rely on subsurface scattering approximations based on the use of phase functions – notably, the Henyey-Greenstein phase function and its variations. In this paper, we challenge the generalized use of these approximations, especially for organic materials, and propose the application of a data-oriented approach whenever reliable measured data is available. Our research is supported by comparisons involving the original measured data that motivated the use of phase functions in algorithmic simulations of tissue subsurface scattering. We hope that this investigation will help strengthen the biophysical basis required for the predictable rendering of organic materials.

Keywords biophysically-based rendering · phase function

1 Introduction

Since the beginning of computer graphics in the late 1960s, researchers have been mostly concerned with the process of creating realistic images of the world around us. One of the most important stages of this process is the simulation of light interaction with matter. Efforts in this area resulted in predictable images of inorganic materials. More recently, organic materials, such as plant and human tissues [18, 23, 25, 37, 48], whose scattering behavior is characterized by a highly significant subsurface component, have been carefully rendered to generate believable images. For these materials, however, one may ask a couple of questions. First, are the models of light interaction with organic materials accurate from a biophysical point of view? Second, are these simulations predictive?

In order to answer these questions, one needs to perform comparisons between modeled and measured data. In general, such comparisons are not performed, and the employed validation approach is based solely on visual inspection of the generated images. For applications in several areas (e.g., entertainment and gaming industries) believable images are usually good enough. However, if the models were described by biophysically meaningful parameters and the algorithms and resulting images were accurate representations of light transport processes, the simulations could be used in a predictive manner [17]. This would make the process of realistic image synthesis more intuitive [2]. Furthermore, this biophysically based approach has a broader range of applications, including not only believable picture-making, but also scientific and medical applications such as the noninvasive diagnosis of skin phototraumas and tumors [10, 53].

Accuracy and computational time are often conflicting issues in biophysically based rendering. Although the main goal in this area is the design of accurate and efficient models, sometimes it is difficult to obtain this perfect combination. In order to achieve a higher level of accuracy, it may be necessary to add complexity to a model, which in turn may negatively affect its computational performance. However, this is not always the case. In fact, we are going to show in this paper that one may be able to obtain more accurate and efficient representations of biophysical phenomena in many cases by removing undue complexity.

The core of any rendering algorithm is formed by the scattering functions. These are also called phase functions

when applied to volumetric scattering [15]. The purpose of this paper is to investigate the foundations of subsurface scattering simulations, including the widespread application of the Henyey-Greenstein phase function (henceforth referred to as HGPF) [19] in the modeling of light transport in tissue. We are going to show through comparisons with actual measured data that it negatively affects both accuracy and predictability of subsurface scattering simulations. We will demonstrate that a significant step toward predictive tissue optics models can be given by using experimental data directly, instead of functions which came to play just as an attempt to fit such data.

The remainder of this paper is organized as follows: the next section provides an overview of the HGPF formulation and terminology. Section 3 presents an original chronology of tissue optics research that resulted in the questionable generalized application of HGPF in tissue subsurface scattering simulations. Section 4 describes the experimental investigation setup used to demonstrate the pitfalls of the HGPF approximations and the advantages of a data-oriented approach. Section 5 presents the results of these comparisons and discusses their practical implications. Finally, Section 6 concludes the paper emphasizing the need for a multidisciplinary effort to advance this important area of research.

2 HGPF: formulation and terminology

When light hits a particle with an index of refraction different from that of its environment, the light is scattered. The direction of scattering is characterized by the polar angle θ at which the light is bent and an azimuthal angle β in a plane normal to the direction of incidence (Fig. 1).

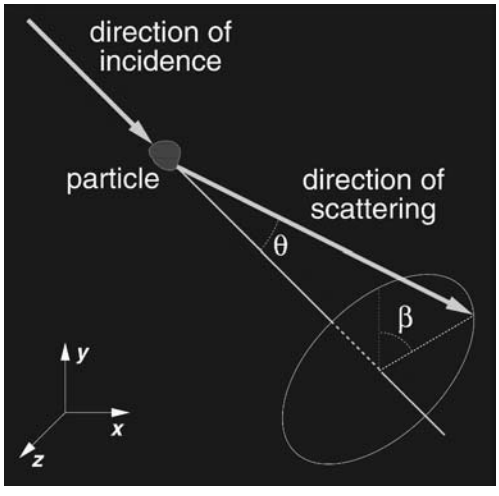

Fig. 1. Sketch describing the scattering angles associated with a phase function $\phi(\theta, \beta)$

A phase function denoted by $\phi(\theta, \beta)$ describes the amount of light scattered from the direction of incidence to the direction of scattering [57], i.e., it represents a single scattering event. The probability of light scattering through an angle θ after n scattering events is given by a multiple-scattered phase function, a concept used by Tessendorf and Wasdon [50] to simulate multiple scattering in clouds, and recently applied by Premoze et al. [44] in the rendering of objects with subsurface scattering.

The name "phase function" has no relation to the phase of the electromagnetic wave (light). It has its origins in astronomy, where it refers to lunar phases [21]. Coincidentally, one of the most widely used phase functions in radiative transfer theory, and the focus of our investigation, the HGPF, was designed for astrophysical applications [19].

The HGPF was presented by Henyey and Greenstein to approximate Mie scattering in their study of diffuse radiation in galaxies [19]. It is important to note, however, that a theoretical derivation for this phase function was not provided by Henyey and Greenstein [19]. The HGPF is given by

$$\phi(g, \theta) = \frac{1 - g^2}{\left(1 + g^2 - 2g\cos\theta\right)^{\frac{3}{2}}}, \tag{1}$$

where the parameter g is defined as the integral over all angles of the phase function multiplied by the cosine of the angle θ. The HGPF is actually a function of *three* parameters: g, θ and β. It just happens that an azimuthal symmetry of the phase function is assumed, i.e., the function is constant with respect to β. Sometimes is convenient to write the HGPF multiplied by $\frac{\gamma}{K}$, where γ represents the spherical albedo [19], and K is a constant that enforces unit area for a probability density function (please refer to the appendix). We choose, in accord with most computer graphics authors, to write the HGPF as described in Eq. 1. By varying parameter g, called the asymmetry factor, in the range $-1 \leq g \leq 1$, it is possible to characterize HGPFs ranging from a completely backward-throwing to a completely forward-throwing form (Fig. 2).

The HGPF as defined in Eq. 1 cannot, however, be used to describe simultaneous forward and backward lobes that are typical in many cases of Mie scattering as well as Rayleigh scattering [62]. For this reason, astrophysicists proposed variations based on the superposition of two HGPFs [27, 55, 62]:

$$\phi(g_1, g_2, \theta, u) = u\phi(g_1, \theta) + (1 - u)\phi(g_2, \theta), \tag{2}$$

where $\phi(g_1, \theta)$ and $\phi(g_2, \theta)$ are of the form given by Eq. 1 and u is a "blending factor" used to weight the two component HGPFs. Figure 3 illustrates three scattering profiles provided by the two-term HGPF.

The asymmetry factor is often called the anisotropy factor. We employ the former term throughout this paper

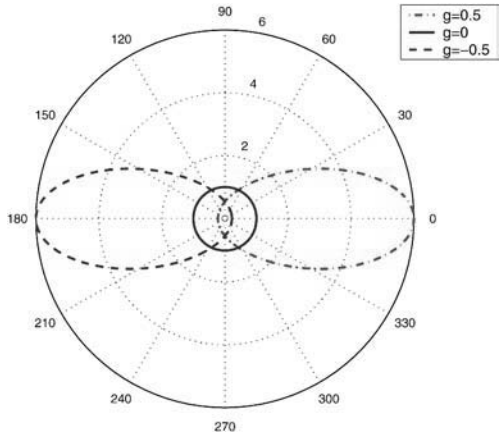

Fig. 2. Scattering diagrams illustrating different scattering profiles provided by the HGPF

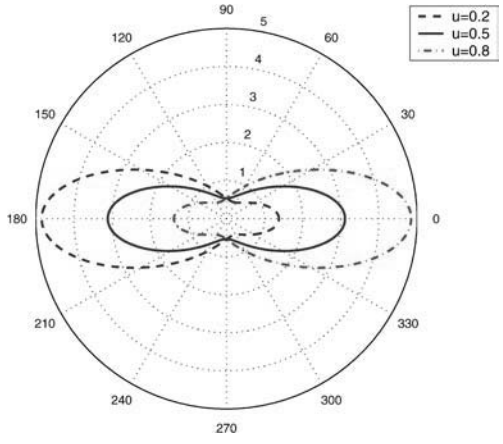

Fig. 3. Scattering diagrams illustrating different scattering profiles provided by the two-term HGPF with $g_1 = 0.5$ and $g_2 = -0.5$

since we consider the use of the term "anisotropy" inappropriate. Recall that the function has no dependence on the azimuthal angle. Furthermore, there is no direct relationship between this parameter and a macroscopic anisotropic behavior of a given material, i.e., a dependence on both the polar and the azimuthal angles measured from the material's normal and used to define the direction of incidence of the incoming light.

3 HGPF in tissue subsurface scattering: chronology and problems

The HGPF is neither based on a mechanistic theory of scattering [22] nor does its asymmetry factor have any biological meaning. Two important questions then come to mind. Why is the HGPF extensively used in rendering of both inorganic and organic materials? What problems may result from its usage? In order to answer these questions, we need to go back in time and track down the sequence of events that culminated in its use in tissue subsurface scattering simulations.

In 1976, bioengineers [40] attempted to use the HGPF to approximate Mie scattering in blood. Their investigation did not show a good agreement between the HGPF approximation and the experimental data, however.

Later on, Bruls and van der Leun [8] performed goniometric measurements of the scattering profile of two types of skin tissues – namely, the stratum corneum and the epidermis – obtained from real specimens. These tissues are characterized as forward-scattering media [1]. In the former, this behavior is due to the alignment of the fibers, while in the latter, it is due to Mie scattering caused by particles that are approximately the same size of the wavelength of light (e.g., cell organelles) [8]. The average thicknesses of the stratum corneum and epidermis samples used in the measurements performed by Bruls and van der Leun [8] were 26 μm and 69 μm, respectively [7].

For the visible region of the light spectrum, the measurements were performed at 436 nm and 546 nm (Table 1) with an angle of incidence of 0°. Although some light might be reflected on the surface due to Fresnel effects, due to the normal angle of incidence and the refractive index differences, this portion of reflected light was considered negligible [6, 7]. Also, because of the approximate match of the refractive indices of the specimens and the sample carriers, the refraction of the transmitted light due to Fresnel effects was also assumed to be negligible [8].

The resulting data correspond to the amount of radiation transmitted into a solid angle $\Delta\omega$, centered around the direction given by θ, as a fraction of the total radiation transmitted in perpendicular irradiation. The measured scattering distributions were in the range given by

Table 1. Scattering profiles of stratum corneum and epidermis tissues measured at 436 nm and 546 nm, and presented in terms of the cumulative fractions (%), $C(\theta)$, of radiation transmitted within a certain angle θ with respect to the tissue's normal (redrawn with permission from [8] for completeness)

Angle	Stratum corneum		Epidermis	
θ	436 nm	546 nm	436 nm	546 nm
2.5°	17.6	20.6	2.6	4.0
7.5°	55.2	60.2	16.1	22.5
12.5°	70.9	75.2	30.8	39.7
17.5°	79.1	82.3	43.6	52.5
22.5°	84.1	86.5	54.5	62.4
27.5°	87.6	89.4	63.9	70.2
32.5°	90.3	91.5	71.9	76.7
37.5°	92.5	93.4	79.0	82.4
42.5°	94.4	95.0	85.0	87.2
47.5°	96.1	96.5	90.1	91.4
52.5°	97.6	97.8	94.3	94.9
57.5°	99.0	99.0	97.8	97.9
62.5°	100.0	100.0	100.0	100.0

$0° \leq \theta \leq 62.5°$. The missing fractions, beyond 62.5°, were considered negligible by Bruls and van der Leun [8], and the cumulative fractions of the transmitted energy were expressed as

$$C_i(\theta) = \frac{\int_{0°}^{\theta_i} I(\theta) \sin\theta d\theta}{\int_{0°}^{62.5°} I(\theta) \sin\theta d\theta} \times 100\%, \quad (3)$$

where I corresponds to the transmitted radiant intensity, and $\theta_i = 5i + 2.5°$ for $i = 0, \ldots, 12$.

It is important to note that the scattering profile of skin tissues, especially the epidermis, is relevant not only for simulation of skin appearance, but also for the visual diagnosis of medical conditions such as skin melanoma [10, 53]. In their paper, Bruls and van der Leun [8] suggested the measured scattering profile of these tissues could be approximated by single-particle phase functions:

> *We compared epidermal profiles with results from multiple scattering theory. Van de Hulst (1980) provides elaborate computations of scattering profiles of layers filled with particles, on the basis of a single-particle scattering phase function that ranges from diffuse to very forward-oriented. Our epidermal profiles are compatible with profiles from his Table 35.*

The table from van de Hulst [56] mentioned above corresponds to the HGPF. In 1987, Jacques et al. [22] followed Bruls and van der Leun's suggestion, and tried to approximate the measured scattering profile of another skin tissue, namely the dermis, using HGPF with $g = 0.81$. Yoon et al. [64] used similar g values for a human aorta. The experiments on the dermis and aorta tissues were aimed at specific medical applications and conducted with a HeNe laser (632.8 nm). Motivated by these works, Prahl [42] proposed a Monte Carlo-based algorithm to model light transport in tissue during laser irradiation. Although this Monte Carlo-based approach was used before to study light propagation in tissue [61], Prahl's algorithmic formulation, to the best of our knowledge, was the first proposed to use the HGPF to compute the scattering of photons in organic tissues. In order to compute the trajectories of the scattered photons, Prahl [42] used a warping function provided by Witt [62], which was obtained by setting

$$\xi_1 = 2\pi \int_{-1}^{\cos\theta} \phi\big(\cos\theta', g\big) d\cos\theta', \quad (4)$$

and finding upon integration that

$$\cos\theta = \frac{1}{2g}\left\{1 + g^2 - \left[\frac{1-g^2}{1-g+2g\xi_1}\right]^2\right\}, \quad (5)$$

where ξ_1 is a uniformly distributed random number on the interval [0, 1]. An alternative original derivation of this warping function is given in the appendix. For symmetric scattering ($g = 0$) the expression $\cos\theta = 2\xi_1 - 1$ should be used [43]. Since an azimuthal symmetry of the phase function is assumed, the azimuthal angle can be generated using $\beta = 2\pi\xi_2$, where ξ_2 is a random number uniformly distributed on the interval [0, 1].

In 1989, biomedical researchers [58] attempted to fit the HGPF to the goniometric measurements of Bruls and van der Leun [8], and used a least-squares method to determine suitable values for g. After that, it was assumed that the HGPF could be used to approximate the scattering profile of organic materials regardless of wavelength, and only a few works questioned its applicability for biological cells [12, 36]. In fact, the use of HGPF in analytical and algorithmic subsurface scattering simulation became widespread in many areas involving tissue optics [53], and new comprehensive goniometric measurements for tissue subsurface scattering were not performed.

In 1993, graphics researchers [18] introduced the algorithmic formulation for the simulation of tissue subsurface scattering proposed by Prahl [42] to the graphics literature. This included the use of the HGPF described above. In their examples, Hanrahan and Krueger used $g = 0.81$ for the dermis and $g = 0.79$ for the epidermis. They did not include the stratum corneum in their skin representation. Since then, the HGPF has also been used in computer graphics applications involving subsurface scattering simulations [24, 25, 37, 41, 44, 48].

Are there indeed any problems with this use of HGPF in tissue subsurface scattering simulations? First, recall that the asymmetry factor g has no direct connection to the underlying biophysical phenomena. Second, as described above, the HGPF was initially meant to be used in tissue optics just as a function to fit multiple scattering data of skin measured at specific wavelengths. As we are going to show in the following sections, the HGPF approximations deviate from the measured data.

The suitability of HGPF approximations is even more questionable when they are used to describe the subsurface behavior of materials characterized by a dominant reflective-refractive scattering (caused by internal structures much larger than the wavelength of light) such as plant tissues [16]. In these applications the selection of values for the asymmetry factor g is made on a trial-and-error basis, and it has neither an empirical nor a theoretical foundation. For example, Hanrahan and Krueger [18], referring to the work by Ma et al. [33], used $g = 0.3$ in their simulations of internal scattering of plant leaves. It is important to note that the experiments performed by Ma et al. involved a single-wavelength laser (632.8 nm), and, to the best of our knowledge, did not include the selection of biologically plausible values for asymmetry factors. In this case, a simple cosine distribution would be closer to the real thing than the use of the HGPF, since light is quickly randomized within plant tissues [5, 54].

As another example, Jensen et al. [25] used $g = 0.85$ for the whole skin. A single value/or the whole skin, i.e., specific values for each constituent tissue are not considered. We infer that this value comes from a paper that followed Bruls and van der Leun since no direct reference was provided by Jensen et al. [25]. In a recent paper, Jensen and Buhler [23] used the HGPF with the asymmetry values provided by van Gemert et al. [58]. Another question then comes to mind: why can one not use the actual data from Bruls and van der Leun [8]? For example, Krishnaswamy and Baranoski [28] used the values provided by Bruls and van der Leun in the development of a biophysically based spectral skin model (BioSpec) [28], whose reflectance and transmittance results show a good quantitative and qualitative agreement with skin spectral data for both the stratum corneum and epidermal tissues. In the case of deeper dermal layers, the spatial distribution of the scattered light quickly becomes diffuse after the first interactions [22]. In this case, a simple cosine distribution would also be closer to the real thing than the use of the HGPF [28]. This approach was also used in the BioSpec model. Incidentally, although the near-Lambertian bidirectional transmittance distribution function (BTDF) of the whole skin can be observed in body parts such as ears, eyelids, and fingers, actual measured data is scarce. Figure 4 presents images generated using BioSpec to illustrate the translucency of human skin in a predictive manner – in this case, according to variations in the pigmentation level.

The incorporation of the HGPF in models of light interaction with matter can affect not only transmission, but also reflection of light. Since the HGPF as defined in Eq. 1 cannot be used to describe simultaneous forward and backward lobes, it directly affects the propagation of light in one direction, e.g., upwards. However, algorithmic models [18, 42] can apply the function every time a ray traverses a medium, either upwards or downwards, therefore affecting both reflection and transmission. For models that apply the superposition of HGPFs (Sect. 2), such as the model used by Jensen et al. [24] to simulate wet powdered materials, the combined HGPFs can affect the reflection and the transmission of light at each interaction. Among the powdered materials mention by Jensen et al. are different types of soil such as sand and clay. As stated by Li [32], these phase functions are not derived from physical principles in terms of the physical and geometrical properties of soil particles, and their adjustable nonphysical parameters can be related to the properties of the soil particles only empirically. Hence, models using these phase functions may be used to generate believable images of soils, but not predictable ones.

It is worth noting, however, that for many materials, there is neither measured data available nor an accurate understanding of the underlying physical processes involved in their interaction with light. In these situations, one may need to resort to a level of abstraction that can provide a reasonable approximation. For example, to the best of our knowledge, the scattering data for space nebulae is scarce. In this case, the use of empirical phase functions may be the best approach that one can apply.

In short, we believe that the generalized application of HGPF approximations to any organic tissue and any wavelength may lead to incorrect results, specially using asymmetry factors determined by fitting the HGPF to specific data sets that may have no relationship with the material at hand. Furthermore, we maintain that the use of this function adds undue complexity to algorithmic subsurface scattering simulations when measured data is available. In the following sections, we will show that these simulations can be performed with a higher accuracy-to-time ratio using measured data directly.

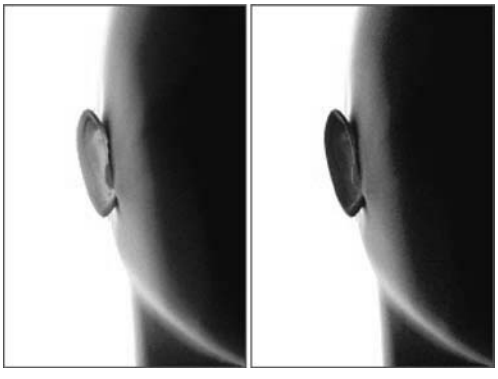

Fig. 4. Images generated using the BioSpec model [28] to illustrate variations in the translucency of skin tissues associated with different levels of pigmentation. Left: lightly pigmented specimen. Right: moderately pigmented specimen

4 Experimental investigation set-up

In order to determine the accuracy of scattering profiles obtained using the HGPF, we compared these profiles with the experimental goniometric data (between 0° and 62.5°) provided by Bruls and van der Leun [8]. For the sake of consistency with the experiments performed by van Gemert et al. [58], we do not take the missing fractions (beyond 62.5°) into account in our experiments. Also, recall that according to estimates provided by Bruls and van der Leun [8], these fractions are negligible.

For the HGPF asymmetry factors, we considered the values determined by van Gemert et al. [58], which have been commonly used in algorithmic subsurface scattering simulations. One might argue that the fitting approach used by van Gemert et al. [58] to determine the g values could be replaced by another approach that could result into better approximations for the profiles. For this reason, we also used g values obtained by applying the RMS error

Table 2. Asymmetry factors obtained by fitting the HGPF to scattering profiles of stratum corneum and epidermis tissues measured at 436 nm and 546 nm

Asymmetry factors	Stratum corneum		Epidermis	
Source	436 nm	546 nm	436 nm	546 nm
RMS error metric	0.935	0.943	0.761	0.821
van Gemert et al.	0.900	0.917	0.748	0.781

metric [15] to the measured data. We have experimented with other error metric approaches, e.g., absolute and relative deviations [4]. We selected the results obtained using the RMS error metric for presentation since the RMS g values provide a closer visual match to the results obtained using the measured data. The asymmetry factors used in our comparisons are presented in Table 2. They correspond to the measured data for the visible range of the light spectrum (436 nm and 546 nm) provided by Bruls and van der Leun [8].

To determine the asymmetry factors, we initially subtracted the consecutive cumulative fractions of the transmitted radiation (Eq. 3) to get $F_\tau^{(i)} = C_i - C_{i-1}$, for $i = 1, \ldots, 12$, and $F_\tau^{(0)} = C_0$. Thus,

$$F_\tau^{(i)} = \frac{\int_{\max(0^\circ,\theta_i-5^\circ)}^{\theta_i} I(\theta)\ \sin\theta d\theta}{\int_{0^\circ}^{62.5^\circ} I(\theta)\ \sin\theta d\theta}, \tag{6}$$

where $\theta_i = 5i + 2.5^\circ$, for $i = 0, \ldots, 12$.

Next, to obtain the HGPF data to be compared to the data from Eq. 6, we computed the following cumulative density function:

$$P(\theta < \theta') = \int_0^{\theta'} \phi_g(g, \theta)\ \sin\theta d\theta, \tag{7}$$

and we obtained

$$C_{g,i} = \frac{P(\theta < \theta_i)}{P(\theta < 62.5^\circ)}, \tag{8}$$

where $\theta_i = 5i + 2.5^\circ$, for $i = 0, \ldots, 12$. We then performed the operation $F_\tau^{(g,i)} = C_{g,i} - C_{g,i-1}$ for $i \geq 1$ and $F_\tau^{(g,0)} = C_{g,0}$.

The RMS error metric $\epsilon_{RMS}(g)$ used to compare the $F_\tau^{(i)}$ and the $F_\tau^{(g,i)}$, for $i = 0, \ldots, 12$, is given by

$$\epsilon_{RMS}(g) = \sqrt{\frac{1}{m}\sum_{i=0}^{m-1}\left(F_\tau^i - F_\tau^{(g,i)}\right)^2}, \tag{9}$$

where $m = 13$. We applied the Nelder-Mead simplex search algorithm [30] to minimize $\epsilon_{RMS}(g)$ over $g \in [-1, 1]$ to obtain the most suitable asymmetry factor.

We believe that a data-oriented approach provides approximations with a higher accuracy-to-time ratio. In order to confirm this assertion, we implemented a randomized table look-up algorithm. The scattering angles are stored in a table, whose access indices correspond to the measured fractions of scattered radiation. For each photon, we generate a uniformly distributed random number on the interval [0, 1]. We then multiply this number by the table size. The integer part of the resulting value is used to access the corresponding scattering angle stored in the table. The table size is limited by the granularity of the measured goniometric data, which consists of values with one decimal digit accuracy (Table 1). Thus, for each wavelength considered, we used a table with 1000 entries. The intermediate data values were obtained through interpolation, another design choice based on the granularity of the measured goniometric data. For the sake of simplicity and due to the lack of information about the scattering behavior between data points, we used linear interpolation.

We performed two sets of experiments. In both sets, we generate N samples (photons) represented by random numbers uniformly distributed on the interval [0, 1].

In the first set (with $N = 10^5$), for each photon, we determined the scattering angle given by Eq. 5 with the g values presented in Table 2 and the scattering angle given by the randomized table look-up technique. The number of samples per measured scattering angle for each approach was recorded and the comparisons were performed. Since the experimental data was limited to 62.5°, the scattering angles given by the HGPF beyond this value were discarded and not taken into account into the sample summations.

The second set of experiments (with $N = 10^6$) followed a similar protocol. It was performed through the implementation of a virtual goniometer [29], which was used to compute the BTDF (bidirectional transmittance distribution function) associated with the scattering profiles obtained using the HGPF and the randomized table look-up technique. Since an azimuthal symmetry of the phase function is assumed (see Sect. 2), the BTDF values were computed on the plane given by the incident light and the tissue's normal. The BTDF values corresponding to the measured data, denoted by f_τ^i, for $i = 0, \ldots, 12$, were calculated using

$$f_t(\vec{\omega}_i, \vec{\omega}_t, \lambda) = \frac{F_\tau^{(i)}(\lambda)}{\vec{\omega}_t\ \cos\theta}, \tag{10}$$

where $\vec{\omega}_i$ and $\vec{\omega}_t$ correspond to the incidence and transmissive solid angles, and λ corresponds to the wavelength at which the measurements were performed. Similarly, to compute the BTDF corresponding to HGPF data, we replaced $F_\tau^{(i)}$ by $F_\tau^{(g,i)}$ in the equation above.

It is worth noting that the spatial patterns of light distribution can be more accurately represented by the bidirectional scattering-surface distribution function (BSSDF),

or its components; namely, the bidirectional scattering-surface reflectance-distribution function (BSSRDF) and the bidirectional scattering-surface transmittance-distribution function (BSSTDF) [38]. However, as appropriately mentioned by Glassner [15], the BSSDF is a difficult function to measure, store, and compute with, due its dependency on four parameters: the incidence and outgoing directions, the wavelength, and the position on the surface. For this reason, sometimes it is more practical to make simplifying assumptions about the material in order to obtain a more tractable function. For example, if one assumes that a given material's properties are the same everywhere, the position parameter becomes irrelevant [15]. In this case, one can work with simpler function – namely, the bidirectional surface-scattering distribution function (or simply the BDF) – which can also be decomposed into its two components: BRDF (bidirectional reflectance distribution function) and BTDF. The reason we use BTDF in this investigation instead of BSSTDF is because the original set of subsurface measurements that triggered the generalization of the HGPF did not account for positional variations.

Organic tissues, such as the stratum corneum and epidermis, are usually considered as part of a whole material, i.e., human skin. Moreover, there are other factors affecting subsurface scattering such as the absorption of light by pigments [28]. However, one may use simple abstractions, called "phantom materials," to expand the scope of visual observations. Such abstractions are extensively used in biomedical research [10, 47], and similar abstractions have also being used in computer graphics [2, 3]. In our investigation, these phantom materials are represented by thin translucent sheets with a forward-scattering behavior simulated using the HGPF (with the values given in Table 2) and the randomized table look-up technique. They are illuminated by Lambertian light sources represented by background surfaces. The resulting images were obtained using a standard path-tracing algorithm without postprocessing signal smoothing [15]. We remark that the purpose of these images is just to visually illustrate the spatial patterns of light distribution resulting from the application of the HGPF and the data-driven approach.

5 Results and discussion

The results of the first set of experiments that consider the stratum corneum data are shown in Fig. 5 (top row). As expected, the randomized table look-up technique provides the closest match to the measured data, which can also be observed in Table 3. It is worth noting that the use

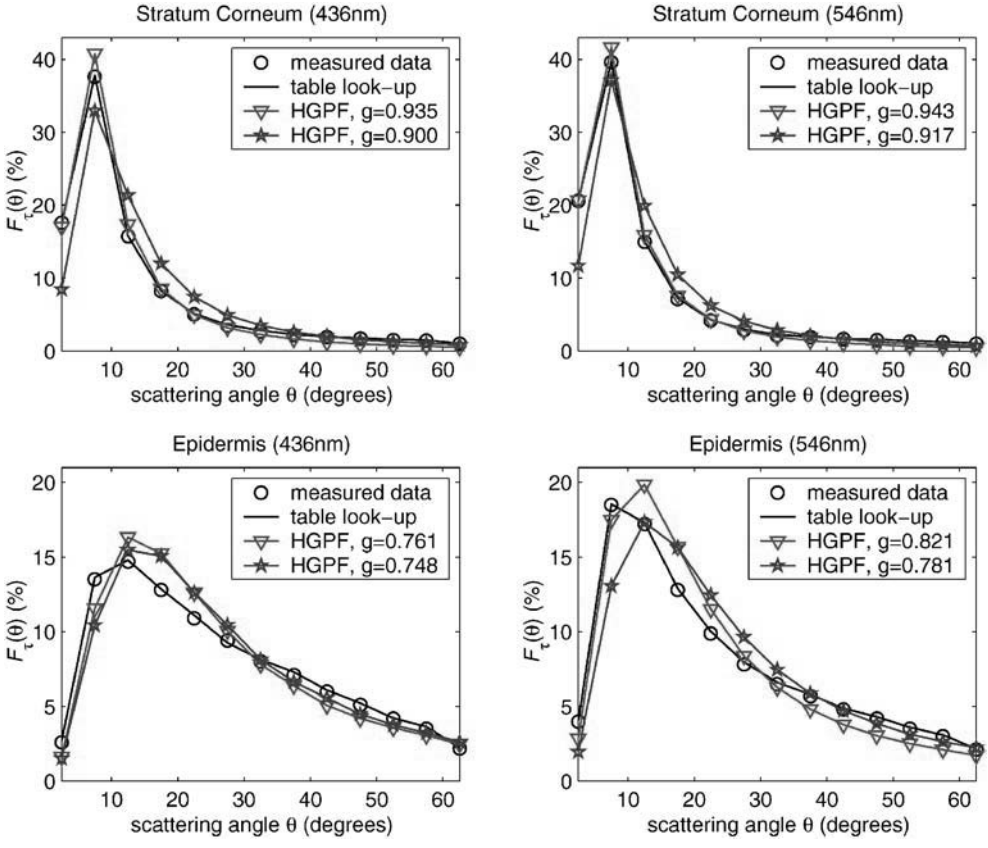

Fig. 5. Comparison between reconstructed transmitted radiation curves and goniometric measured data for the stratum corneum and epidermis tissues

Table 3. Relative error figures – namely, maximum and average values (%) – for the approximation methods (with $N = 10^5$) with respect to the goniometric data for the stratum corneum and epidermis measured at 436 nm and 546 nm

Approximation approach	Stratum corneum				Epidermis			
	436 nm		546 nm		436 nm		546 nm	
	Max.	Avg.	Max.	Avg.	Max.	Avg.	Max.	Avg.
HGPF, with g provided by van Gemert et al.	51.96	27.08	47.71	27.76	42.40	14.04	51.24	16.09
HGPF, with g provided by RMS error metric	53.03	23.08	52.79	21.90	35.24	14.57	30.02	18.43
randomized table look-up	7.22	3.32	8.48	4.17	3.45	1.56	3.25	1.70

of asymmetry factors given by the RMS error metric provides a closer approximation than the values provided by van Gemert et al. [58], which have been used in computer graphics simulations [18, 23].

The results of the first set of experiments that consider the epidermis data are given in Fig. 5 (bottom row). In this case, the disparity between the HGPF approximations and the measured data, which increases for data measured at 546 nm, can be observed. Again, a more accurate approximation is provided by the randomized table look-up technique. It introduces even smaller errors with respect to the epidermis data set, which can also be observed in Table 3.

Figures 6 and 7 present the results of the second set of experiments with stratum corneum data. They show that the quantitative discrepancies between BTDF values

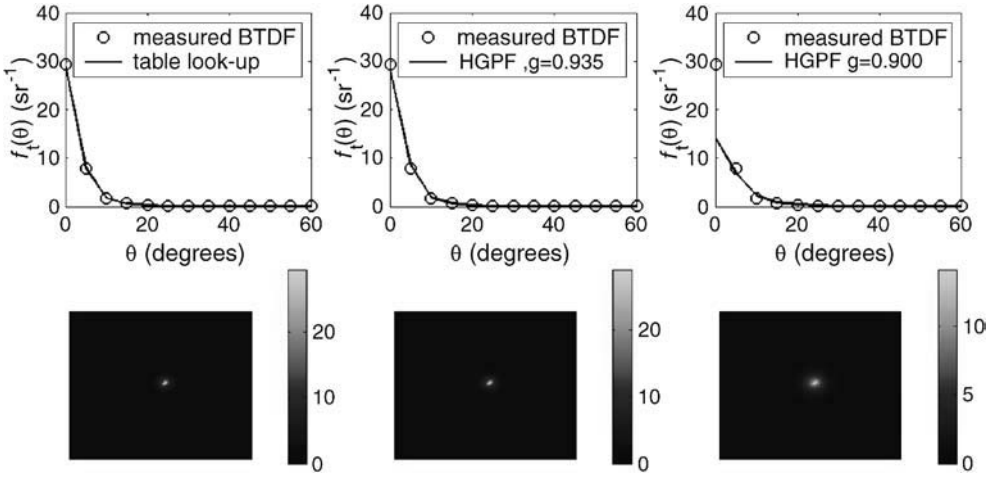

Fig. 6. Reconstructed BTDF values for the stratum corneum tissue at 436 nm. Left: table look-up. Middle: HGPF (with RMS g). Right: HGPF (with g provided by van Gemert et al. [58]). Top row: Cartesian plot. Bottom row: orthographic projection of the scattering diagram

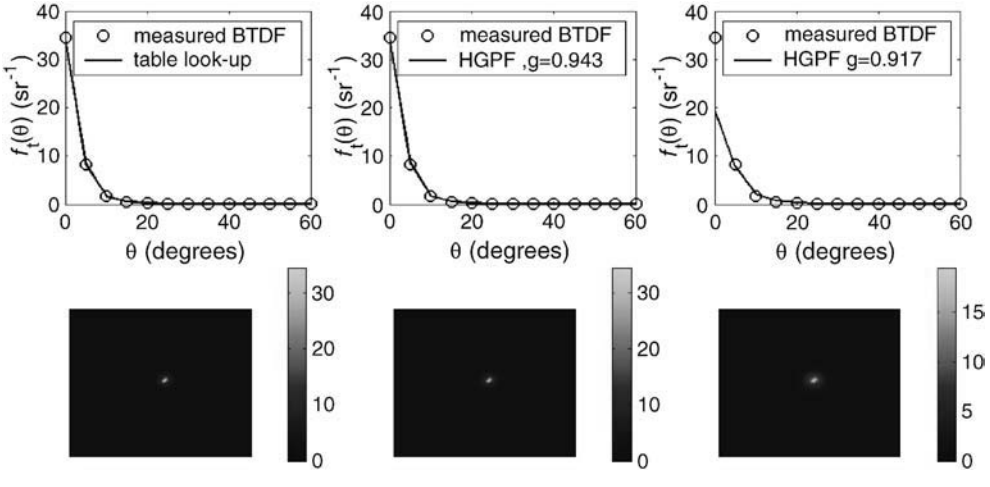

Fig. 7. Reconstructed BTDF values for the stratum corneum tissue at 546 nm. Left: table look-up. Middle: HGPF (with RMS g). Right: HGPF (with g provided by van Gemert et al. [58]). Top row: Cartesian plot. Bottom row: orthographic projection of the scattering diagram

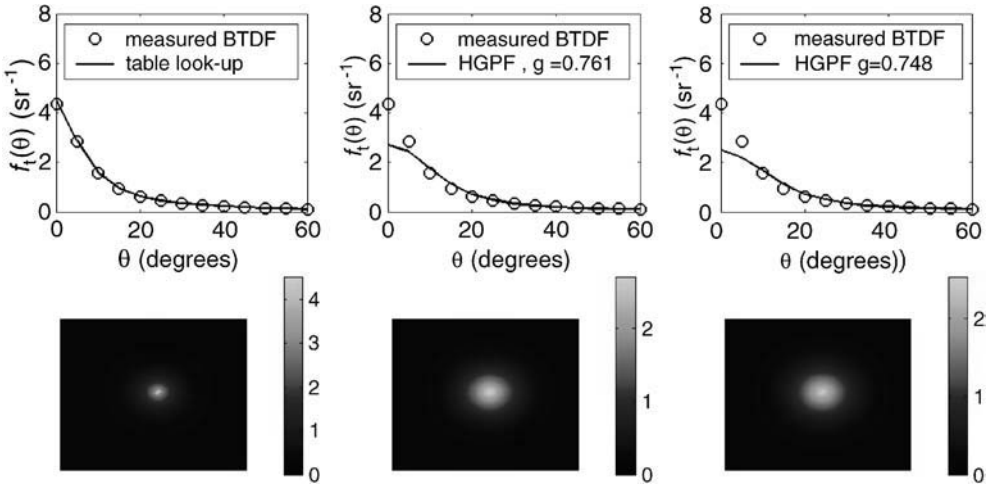

Fig. 8. Reconstructed BTDF values for the epidermis tissue at 436 nm. Left: table look-up. Middle: HGPF (with RMS g). Right: HGPF (with g provided by van Gemert et al. [58]). Top row: Cartesian plot. Bottom row: orthographic projection of the scattering diagram

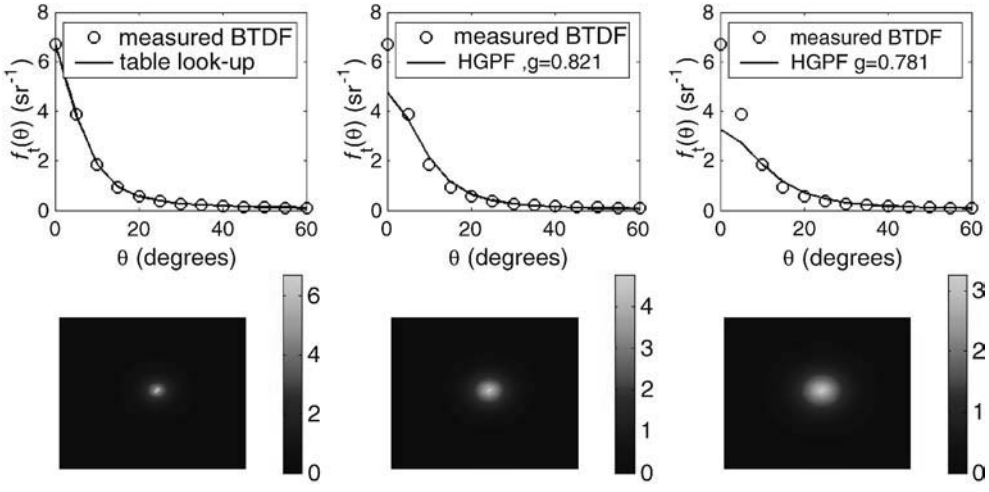

Fig. 9. Reconstructed BTDF values for the epidermis tissue at 546 nm. Left: table look-up. Middle: HGPF (with RMS g). Right: HGPF (with g provided by van Gemert et al. [58]). Top row: Cartesian plot. Bottom row: orthographic projection of the scattering diagram

obtained using the randomized table look-up and the reconstructed BTDF values obtained using the HGPF are small, with closer approximations being obtained using asymmetry factors provided by the RMS error metric.

The results of the second set of experiments with epidermis data, which are presented in Figs. 8 and 9, show noticeable quantitative and qualitative discrepancies between the BTDF values obtained using the randomized table look-up and the BTDF values obtained using the HGPF. For these experiments, closer approximations were also obtained using asymmetry factors provided by the RMS error metric.

In summary, our experiments indicate that the randomized table look-up provides a more accurate agreement with the measured data. The magnitude of the discrepancies between this approach and the HGPF approach may, however, have a different significance depending on the application. For rendering frameworks aimed at scientific and medical applications, it is clearly relevant. For example, the epidermis contains an important skin pigment, melanin. The amount of light absorbed by this pigment affects not only the skin's appearance [52], but also the visual diagnosis of medical conditions such as melanomas at early stages [10]. This amount depends on the path-length of the incoming photons, which is in turn affected by the tissue's scattering properties. In theory, one could select another phase function to fit the scattering data, e.g., the Reynolds-McCormick [45, 49] or the Dunn and Richards-Kortum [12, 36] phase functions. The generalized used of these functions, however, has the same drawbacks as the generalized use of the HGPF.

For rendering frameworks aimed at believable picture-making applications, the visual effects caused by the different approaches may become more pronounced or negligible depending on the illumination conditions (e.g., collimated or diffuse incident beams), the structural characteristics of the materials (e.g., thickness), and perception issues associated with the human visual system [17]. Figures 10 to 12 illustrate this aspect through images of phantom materials generated using the stratum corneum and

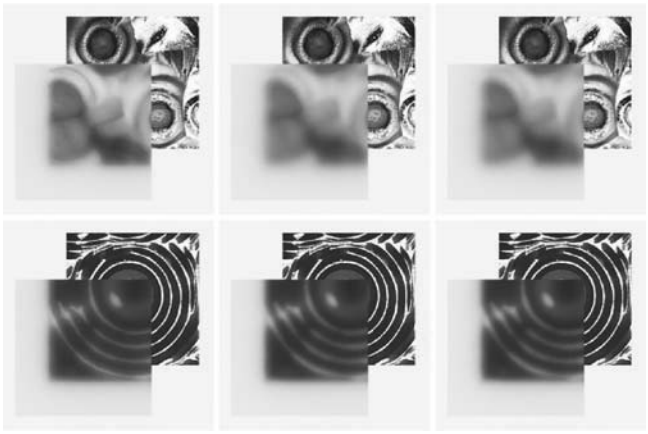

Fig. 10. Images of a phantom material with a scattering behavior simulated using data corresponding to the scattering behavior of the stratum corneum tissue measured at 436 nm (top row) and 546 nm (bottom row). Left column: applying the randomized table look-up. Middle column: applying the HGPF with the asymmetry factors provided by the RMS error metric. Right column: applying the HGPF with the asymmetry factors provided by van Gemert et al. [58]. Surfaces are separated by 0.9 length units

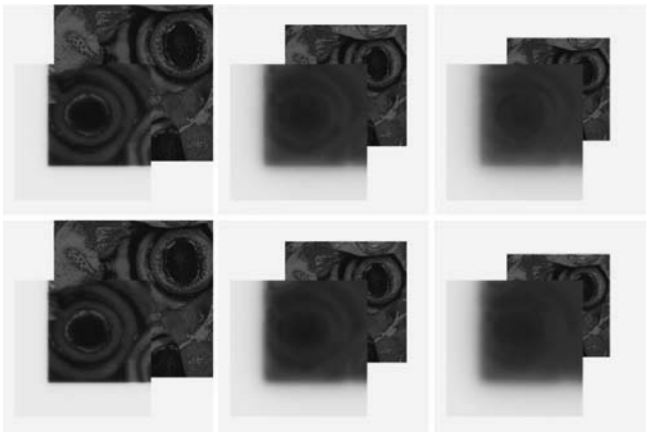

Fig. 11. Images of a phantom material with a scattering behavior simulated using data corresponding to the scattering behavior of the stratum corneum tissue measured at 546 nm. Top row: applying the randomized table look-up. Bottom row: applying the HGPF with the asymmetry factor provided by the RMS error metric. The surfaces are separated by 0.2 (left column), 1.2 (middle column) and 1.8 (right column) length units

the epidermis data respectively. For example, although the experiments presented earlier indicated small discrepancies between the approximation approaches with respect to the stratum corneum data, the images shown in Fig. 10 present remarkable differences in terms of the phantom material's translucency. Such differences can vary depending on, for instance, the distance between the materials' interfaces (which, for an actual tissue, may be associated

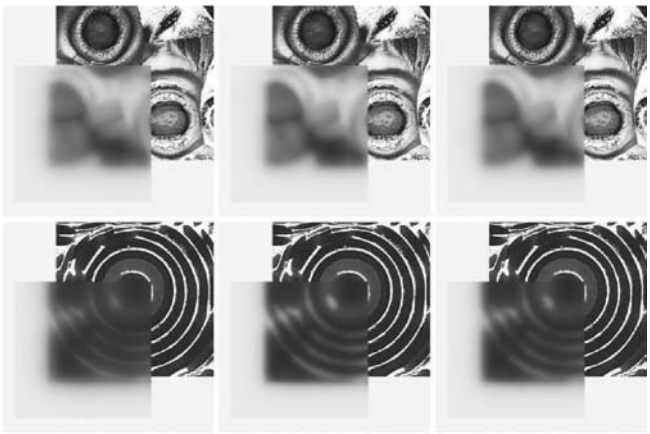

Fig. 12. Images of a phantom material with a scattering behavior simulated using data corresponding to the scattering behavior of the epidermis tissue measured at 436 nm (top row) and 546 nm (bottom row). Left column: applying the randomized table look-up. Middle column: applying the HGPF with the asymmetry factors provided by the RMS error metric. Right column: applying the HGPF with the asymmetry factors given by van Gemert et al. [58]. Surfaces are separated by 0.3 length units

with its thickness) as illustrated in Fig. 11. On the other hand, despite the evident quantitative and qualitative discrepancies between the approximation approaches with respect to the epidermis data verified in the experiments presented earlier, the images present in Fig. 12 (top row) do not present noticeable differences in terms of the phantom material's translucency.

Regarding the computational costs of each approach, recall that the HGPF formulation includes an expensive fractional exponentiation. For example, for the SGI MIPS R14000 processors used in our experiments, this operation is performed five times slower than a randomized table look-up operation. On the other hand, the data-oriented approach requires additional storage space. For instance, the tables used in our experiments occupy 36 kB of memory. Taking into account the relatively large amount of memory available in modern computers and their decreasing price, one may consider this figure quite acceptable. Hence, even for these cases, where the HGPF approximation provides a good match to the measured data, a familiar question resurfaces. Why not use the actual data directly? It is less expensive, the results are more accurate, and the simulation is not controlled by an arcane parameter with no biological basis, which is a crucial criterion to obtain predictable images as illustrated in the development of the BioSpec model [28].

As large multispectral databases become available, memory space may become an issue, and the table size may slow down the simulations, since it can potentially cause many memory swaps. In these situations, numerical techniques, such as principal component analysis (PCA) [26], could be used to reduce the dimensionality

of such databases as it has been done in colorimetry for many years [20, 59]. These techniques not only provide compact databases, but also support the fast addition of new spectral data.

We remark that besides the direct effect on the predictability of algorithmic simulations, the selection of asymmetry factors may have further theoretical implications in tissue subsurface scattering. For example, Jensen and Buhler [23] used a diffusion approximation to improve the efficiency of their subsurface scattering simulations. They state that this approximation has been shown by Furutso [14] to be accurate when $\frac{\sigma_a}{\sigma_a+\sigma_s} \ll 1-g^2$, where σ_a and σ_s correspond to the material's absorption and scattering coefficients, respectively. Clearly, in order to apply this relationship, one needs to know the values of its terms, which in turn come from measured data, especially the asymmetry factor g. As shown by our experiments, the value of g may result from a fitting approach that does not match the measured data accurately, i.e., it may itself be an approximation.

Finally, during this investigation, we unveiled two additional accuracy issues related to the application of the diffusion approximation [23] to describe the subsurface scattering of organic materials – in particular, human skin tissues. First, the diffusion approximation is not suitable when the scattering is mostly in the forward direction [13, 14, 63]. As we have shown in this paper, the measurements performed by Bruls and van der Leun [8] demonstrate that both the stratum corneum and the epidermis tissues are highly forward-scattering media. Second, the diffusion theory is not applicable when the absorption coefficient is not significantly smaller than the scattering coefficient for turbid media [46, 49, 63]. Recall that human skin is characterized by the presence of pigments [28, 39, 51] such as melanin particles, which have a significant absorption cross-section [9].

6 Conclusion and future work

Phase functions, such as the HGPF and its variations, were originally used in tissue subsurface scattering simulations to fit data measured at specific wavelengths. Since then, their application has been extended to different organic materials despite the lack of supporting measured data and the fact that their parameters have no biological meaning. The investigation described in this paper demonstrates that a data-oriented approach increases the accuracy-to-time ratio of algorithmic subsurface scattering simulations and contributes to their predictability, since the simulations are no longer controlled by arcane parameters.

Our investigation also highlights a key issue in biophysically based predictive rendering – namely, the shortage of reliable measured data. Many computer graphics researchers have been working to minimize this problem [11, 17, 31, 34, 35, 60], and a substantial amount of goniometric surface data has been collected and analyzed. Besides being scarcer, goniometric subsurface data may also contain some degree of random noise, which is usually not filtered out by the approximation methods. Therefore, in order to develop predictive subsurface scattering algorithms, we believe that efforts should also be focused on the reliable multispectral measurement of subsurface scattering.

Acknowledgement The authors would like to thank Dr. Wiel A. G. Bruls and Dr. Jan C. van der Leun for their valuable feedback and for making the results of their seminal research work available to the scientific community. Thanks are also due to David Malin for granting us access to his crystal micrographs used as background in our testing images, and the anonymous reviewers for their useful comments and suggestions. The work presented in this paper was supported by the Natural Sciences and Engineering Research Council of Canada (NSERC grant 238337) and the Canada Foundation for Innovation (CFI grant 33418).

Appendix: HGPF warping function

The HGPF, ϕ, is a function of *two* angles: θ and β. That is, $\phi/\int_S \phi$ is the probability density function over the entire sphere, S. Note that $\phi/\int_0^\pi \phi(\theta)d\theta$ is *not* the probability density function for θ over $[0, \pi]$. Since an azimuthal symmetry of the phase function is assumed, i.e., the function is constant with respect to β, the azimuthal angle can be generated using $2\pi\xi_2$, where ξ_2 is a random number uniformly distributed on the interval [0, 1]. To generate θ, we need to invert the cumulative density function for θ: $P(\theta < \theta')$. This can be expressed as

$$P(\theta < \theta') = \frac{1}{K}\int_{\theta<\theta'} \phi(\theta, \beta)d\omega, \tag{11}$$

where $K = \int_S \phi(\theta, \beta)d\omega$ is the constant that enforces unit area for probability density.

Expanding Eq. 11 yields

$$\begin{aligned} P(\theta < \theta') &= \frac{1}{K}\int_0^{2\pi}\int_0^{\theta'} \frac{1-g^2}{\left(1+g^2-2g\cos\theta\right)^{3/2}} \sin\theta\, d\theta\, d\beta \\ &= \frac{1-g^2}{K}\int_0^{2\pi} d\beta \int_0^{\theta'} \frac{\sin\theta\, d\theta}{\left(1+g^2-2g\cos\theta\right)^{3/2}} \\ &= \frac{2\pi}{K}\left(1-g^2\right)\int_0^{\theta'} \frac{\sin\theta\, d\theta}{\left(1+g^2-2g\cos\theta\right)^{3/2}}. \end{aligned}$$

Let $u = 1+g^2-2g\cos\theta$. Then $du = 2g\sin\theta\, d\theta$ and u ranges from $1+g^2-2g = (1-g)^2$ to $1+g^2-2g\cos\theta'$ as θ ranges from 0 to θ'.

Now, we have

$$P(\theta < \theta') = \frac{\pi}{Kg}\left(1-g^2\right)\int_{(1-g)^2}^{1+g^2-2g\cos\theta'} u^{-\frac{3}{2}}\,du$$
$$= \frac{-2\pi}{Kg}\left(1-g^2\right)u^{-\frac{1}{2}}\Big|_{(1-g)^2}^{1+g^2-2g\cos\theta'},$$

which results in

$$P(\theta < \theta') = \frac{2\pi}{Kg}\left(1-g^2\right)\left(\frac{1}{1-g} - \frac{1}{\sqrt{1+g^2-2g\cos\theta'}}\right). \tag{12}$$

Noting that $P(\theta < \pi) = 1$, we can derive K as follows:

$$\begin{aligned}
K &= \frac{2\pi}{g}\left(1-g^2\right)\left(\frac{1}{1-g} - \frac{1}{\sqrt{1+g^2-2g\cos\pi}}\right)\\
&= \frac{2\pi}{g}\left(1-g^2\right)\left(\frac{1}{1-g} - \frac{1}{\sqrt{1+g^2+2g}}\right)\\
&= \frac{2\pi}{g}\left(1-g^2\right)\left(\frac{1}{1-g} - \frac{1}{\sqrt{(1+g)^2}}\right)\\
&= \frac{2\pi}{g}\left(1-g^2\right)\left(\frac{1}{1-g} - \frac{1}{1+g}\right)\\
&= \frac{2\pi}{g}\left(1-g^2\right)\frac{1+g-(1-g)}{1-g^2}\\
&= \frac{2\pi}{g}\cdot 2g\\
&= 4\pi.
\end{aligned}$$

Substituting back into (12) yields

$$P(\theta < \theta') = \frac{1-g^2}{2g}\left(\frac{1}{1-g} - \frac{1}{\sqrt{1+g^2-2g\cos\theta'}}\right). \tag{13}$$

To generate θ', we let $P(\theta < \theta') = \xi_1$, where ξ_1 is a uniformly distributed random number on the interval [0, 1], and solve for θ'. Thus,

$$\begin{aligned}
&\xi_1 = \frac{1-g^2}{2g}\left(\frac{1}{1-g} - \frac{1}{\sqrt{1+g^2-2g\cos\theta'}}\right)\\
&\Rightarrow \frac{1}{\sqrt{1+g^2-2g\cos\theta'}} = \frac{1}{1-g} - \frac{2g\xi_1}{1-g^2}\\
&\Rightarrow \frac{1}{\sqrt{1+g^2-2g\cos\theta'}} = \frac{1+g-2g\xi_1}{1-g^2}\\
&\Rightarrow \sqrt{1+g^2-2g\cos\theta'} = \frac{1-g^2}{1+g-2g\xi_1}\\
&\Rightarrow 1+g^2-2g\cos\theta' = \left(\frac{1-g^2}{1+g-2g\xi_1}\right)^2\\
&\Rightarrow \cos\theta' = \frac{1}{2g}\left(1+g^2-\left(\frac{1-g^2}{1+g-2g\xi_1}\right)^2\right).
\end{aligned}$$

In summary, to generate a random direction distributed according to the HGPF and represented by the pair (θ, ϕ), we can use the following warping function:

$$(\theta, \beta) = \tag{14}$$
$$\left(\cos^{-1}\left(\frac{1}{2g}\left\{1+g^2-\left[\frac{1-g^2}{1+g-2g\xi_1}\right]^2\right\}\right), 2\pi\xi_2\right).$$

References

1. Anderson RR, Parrish JA (1981) The optics of human skin. J Invest Dermatol 77(1):13–19
2. Arvo JR (1995) Analytic methods for simulated light transport. Dissertation, Yale University
3. Arvo JR (1995) Applications of irradiance tensors to the simulation of non-lambertian phenomena. In: SIGGRAPH, Annual Conference Series, pp 335–342
4. Baranoski GVG, Krishnaswamy A, Kimmel B (2003) Revisiting the foundations of subsurface scattering. Technical Report CS-2003-45, School of Computer Science, University of Waterloo
5. Baranoski GVG, Rokne JG (2004) Light interaction with plants: a computer graphics perspective. Horwood, Chichester
6. Bruls WAG, van der Leun JC (1982) The use of diffuser in the measurement of transmission of human epidermal layers. Photochem Photobiol 36(6):709–713
7. Bruls WAG, Slaper H, van der Leun JC, Berrens L (1984) Transmission of human epidermis and stratum corneum as a function of thickness in the ultraviolet and visible wavelengths. Photochem Photobiol 40(4):485–494
8. Bruls WAG, van der Leun JC (1984) Forward scattering properties of human epidermal layers. Photochem Photobiol. 40(2):231–242
9. Chedekel MR (1995) Photophysics and photochemistry of melanin. In: Chedekel MR, Zeise L, Fitzpatrick TB (eds) Melanin: its role in human photoprotection. Valdenmar, Overland Park, pp 11–22
10. Cotton SD (1997) A noninvasive skin imaging system. Technical Report CSR-97-03, School of Computer Science, The University of Birmingham
11. Dana KJ, van Ginneken B, Nayar SK, Koenderink JJ (1999) Reflectance and texture of real world surfaces. ACM Trans Graph 18(1):1–34
12. Dunn A, Richards-Kortum R (1996) Three-dimensional computation of light scattering from cells. IEEE Select Topics Quantum Electron 2(4):898–905
13. Flock ST, Patterson MS, Wilson BC, Wyman DR (1989) Monte Carlo modeling of light propagation in highly scattering tissues – I: Model predictions and comparison with diffusion theory. IEEE Trans Biomed Eng 36(12):1162–1168
14. Furutso K (1980) Diffusion equation derived from space-time transport equation. J Opt Soc Am 70(4):360–366
15. Glassner AS (1995) Principles of digital image synthesis. Kaufmann, San Francisco
16. Govaerts YM, Jacquemoud S, Verstraete M, Ustin SL (1996) Three-dimensional radiation transfer modeling in

a dycotyledon leaf. Appl Opt 35(33):6585–6598
17. Greenberg DP, Arvo J, Lafortune E, Torrance KE, Ferwerda JA, Walter B, Trumbore B, Shirley P, Pattanaik S, Foo S (1997) A framework for realistic image synthesis. In: SIGGRAPH, Annual Conference Series, pp 477–494
18. Hanrahan P, Krueger W (1993) Reflection from layered surfaces due to subsurface scattering. In: SIGGRAPH, Annual Conference Series, pp 165–174
19. Henyey LG, Greenstein JL (1941) Diffuse radiation in the galaxy. Astrophys J 93:70–83
20. Imai FH, Tsumura N, Haneishi H, Miyake Y (1996) Principal component analysis of skin color and its application to colorimetric reproduction on CRT display and hardcopy. J Image Sci Technol 40(5):422–430
21. Ishimaru A (1997) Wave propagation and scattering in random media, volume 1, 2nd edn. IEEE Press, New York
22. Jacques SL, Alter CA, Prahl SA (1987) Angular dependence of HeNe laser light scattering by human dermis. Lasers Life Sci 1(4):309–333
23. Jensen HW, Buhler J (2002) A rapid hierarchical rendering technique for translucent materials. In: SIGGRAPH, Annual Conference Series, pp 576–581
24. Jensen HW, Legakis J, Dorsey J (1999) Rendering of wet materials. In: Lischinski D, Larson GW (eds) Rendering Techniques 1999, Proceedings of the 10th Eurographics Rendering Workshop, Granada. Springer, Berlin Heidelberg New York, pp. 281–289
25. Jensen HW, Marschner SR, Levoy M, Hanrahan P (2001) A practical model for subsurface light transport. In: SIGGRAPH, Annual Conference Series, pp 511–518
26. Jolliffe IT (2002) Principal component analysis, 2nd edn. Springer, Berlin Heidelberg New York
27. Kattawar GW (1975) A three-parameter analytic phase function for multiple scattering calculations. J Quant Spectrosc Radiat Transfer 15:839–849
28. Krishnaswamy A, Baranoski GVG (2004) A biophysically based spectral model of light interaction with human skin. In: Computer Graphics Forum (EUROGRAPHICS Proceedings) 23(3):331–340
29. Krishnaswamy A, Baranoski GVG, Rokne JG (2004) Improving the reliability/cost ratio of goniophotometric measurements. J Graph Tools 9(3):31–51
30. Lagarias JC, Reeds JA, Wright MH, Wright PE (1998) Convergence properties of the Nelder-Mead simplex method in low dimensions. SIAM J Optim 9(1):112–147
31. Lalonde P, Fournier A (1997) Generating reflected directions from BRDF data. In: Computer Graphics Forum (EUROGRAPHICS Proceedings) 16(3):293–300
32. Li Z, Fung AK, Tjuatja S, Gibbs DP, Betty CL, Irons JR (1996) A modeling study of backscattering from soil surfaces. IEEE Trans Geosci Remote Sens 34(1):264–271
33. Ma Q, Nishimura A, Phu P, Kuga Y (1990) Transmission, reflection and depolarization of an optical wave for a single leaf. IEEE Trans Geosci Remote Sens 28(5):865–872
34. Marschner SR, Westin SH, Lafortune EPF, Torrance KE, Greenberg DP (1999) Image-based BRDF measurement including human skin. In: Lischinski D, Larson GW (eds) Rendering Techniques 1999, Proceedings of the 10th Eurographics Rendering Workshop, Granada. Springer, Berlin Heidelberg New York, pp 119–130
35. Matusik W, Pfister H, Brand M, McMillan L (2003) A data-driven reflectance model. ACM Trans Graph 22(3):759–769
36. Mourant JR, Freyer JP, Hielscher AH, Eick AA, Shen D, Johnson TM (1998) Mechanisms of light scattering from biological cells relevant to noninvasive optical-tissue diagnostics. Appl Opt 37(16):3586–3593
37. Ng CS, Li L (2001) A multi-layered reflection model of natural human skin. In: Computer Graphics International 2001, Hong Kong, pp 249–256
38. Nicodemus FE, Richmond JC, Hsia JJ, Ginsberg IW, Limperis T (1992) Geometrical considerations and nomenclature for reflectance. In: Wolff LB, Shafer SA, Healey GE (eds) Physics-based vision principles and practice: radiometry. Jones and Bartlett, Boston, pp 94–145
39. Parsad D, Wakamatsu K, Kanwar AJ, Kumar B, Ito S (2003) Eumelanin and phaeomelanin contents of depigmented and repigmented skin in vitiligo patients. Br J Dermatol 149(3):624–626
40. Petersen GD, McCormick NJ, Reynolds LO (1976) Transport calculations for light scattering in blood. Biophys J 16:199–207
41. Pharr M, Hanrahan P (2000) Monte Carlo evaluation of non-linear scattering equations for subsurface reflection. In: SIGGRAPH, Annual Conference Series, pp 75–84
42. Prahl SA (1988) Light transport in tissue. Dissertation, The University of Texas at Austin
43. Prahl SA, Keijzer M, Jacques SL, Welch AJ (1989) A Monte Carlo model of light propagation in tissue. SPIE Institute Series IS 5:102–111
44. Premoze S, Ashikhmin M, Shirley P (2003) Path integration for light transport in volumes. In: Christensen P, Cohen-Or D (eds) Eurographics Symposium on Rendering, pp 75–84
45. Reynolds LO, McCormick NJ (1980) Approximate two-parameter phase function for light scattering. J Opt Soc Am 7(10):1206–1212
46. Sardar DK, Levy LB (1998) Optical properties of whole blood. Lasers Med Sci 13(2):106–111
47. Shimada M, Yamada Y, Itoh M, Yatagai T (2001) Melanin and blood concentration in human skin studied by multiple regression analysis: experiments. Phys Med Biol 46(9):2385–2395
48. Stam J (2001) An illumination model for a skin layer bounded by rough surfaces. In: Hanrahan PM, Purgathofer E (eds) Rendering Techniques 2001, Proceedings of the 12th Eurographics Rendering Workshop, London. Springer, Berlin Heidelberg New York, pp 39–52
49. Steinke JM, Shepherd AP (1988) Diffusion model of the optical absorbance of whole blood. J Opt Soc Am 5(6):813–822
50. Tessendorf J, Wilson D (1994) Impact of multiple scattering on simulated infrared clod scene images. In: Christensen P, Cohen-Or D (eds) Characterization and propagation of sources and backgrounds. SPIE, Bellingham, pp 75–84
51. Thody AJ, Higgins EM, Wakamatsu K, Ito S, Burchill SA, Marks JM (1991) Pheomelanin as well as eumelanin is present in human dermis. J Invest Dermatol 97(2):340–344
52. Tsumura N, Ojima N, Sato K, Shiraishi M, Shimizu H, Nabeshima H, Akazaki S, Hori K, Miyake Y (2003) Image-based skin color and texture analysis/synthesis by extracting hemoglobin and melanin information in the skin. ACM Trans Graph 22(3):770–779
53. Tuchin V (2000) Tissue optics light scattering methods and instruments for medical diagnosis. SPIE, Bellingham
54. Tucker CJ, Garrat MW (1977) Leaf optical system modeled as a stochastic process. Appl Opt 16(3):635–642
55. Uesugi A, Irvine WM, Kawata Y (1971) Formation of absorption spectra by diffuse reflection from a semi-infinite planetary atmosphere. J Quant Spectrosc Radiat Transfer 11:797–808
56. van de Hulst HC (1980) Multiple light scattering: tables, formulas, and applications, volume 1. Academic Press, New York
57. van de Hulst HC (1981) Light scattering by small particles, 2nd edn. Dover, New York
58. van Gemert MJC, Jacques SL, Sterenborg HJCM, Star WM (1989) Skin optics. IEEE Trans Biomed Eng 36(12):1146–1154
59. Vrhel MJ, Gershon R, Iwan LS (1994) Measurement and analysis of object reflectance spectra. Color Res Appl 19(1):4–9
60. Ward GJ (1992) Measuring and modeling anisotropic reflection. In: Computer Graphics, SIGGRAPH Proceedings, pp 265–272
61. Wilson BC, Adam G (1983) A Monte Carlo model for the absorption and flux distributions of light in tissue. Med Phys 10(6):824–830

62. Witt AN (1977) Multiple scattering in reflection nebulae. I. a Monte Carlo approach. Astrophys J Suppl Ser 15(1):1–6
63. Yoon G, Prahal SA, Welch AJ (1989) Accuracies of the diffusion approximation and its similarity relations for laser irradiated biological media. Appl Opt 28(12):2250–2255
64. Yoon G, Welch AJ, Motamedi M, van Gemert MCJ (1987) Development and application of three-dimensional light distribution model for laser irradiated tissue. IEEE J Quantum Electron QE-23:1721–1733

GLADIMIR V.G. BARANOSKI received a Ph.D. in Computer Science from the University of Calgary in 1998. Currently, he is a faculty member at the School of Computer Science and the leader of the Natural Phenomena Simulation Group at the University of Waterloo. The results of his research on biophysically-based rendering have been made available to the graphics community through the publication of articles in journals and conference proceedings. He has also organized tutorial presentations for conferences (CGI 2000, EUROGRAPHICS (2001 and 2002) and SIGGRAPH (2002 and 2003)), and he has recently authored a book on topics related to his research.

ARAVIND KRISHNASWAMY is a senior software developer and researcher at Inscriber Technology Corporation, where he has been for the last 5 years. He received his BMath in Computer Science from the University of Waterloo in 2002 and is now a candidate for a MMath in Computer Science. His research interests include the biophysically-based simulation of organic materials and natural phenomena.

BRADLEY KIMMEL is currently a masters student at the University of Waterloo. He received his B.Math in computer science and pure mathematics from the University of Waterloo, Canada. The main topic of his research is reflectance models of natural surfaces.